Synaptic element for neuromorphic computing using a magnetic domain wall device with synthetic pinning sites

Jin, Tianli; Gan, Weiliang; Tan, Funan; Sernicola, Nicolo Roberto; Lew, Wen Siang; Piramanayagam, S. N.

2019

Jin, T., Gan, W., Tan, F., Sernicola, N. R., Lew, W. S., & Piramanayagam, S. N. (2019). Synaptic element for neuromorphic computing using a magnetic domain wall device with synthetic pinning sites. Journal of Physics D: Applied Physics, 52(44), 445001-. doi:10.1088/1361-6463/ab35b7

https://hdl.handle.net/10356/141986

https://doi.org/10.1088/1361-6463/ab35b7

Synaptic Element for Neuromorphic Computing Using a Magnetic Domain Wall Device with Synthetic Pinning Sites

Tianli Jin, Weiliang Gan, Funan Tan, N. R. Sernicola, Wen Siang Lew and S.N. Piramanayagam*

Division of Physics and Applied Physics, School of Physical and Mathematical Sciences, Nanyang Technological University, 637371, Singapore

Email: prem@ntu.edu.sg

Abstract:

The ability to make devices that mimic the human brain has been a subject of great interest in scientific research in recent years. Current artificial intelligence algorithms are primarily executed on the von Neumann hardware. This causes a bottleneck in processing speeds and is not energy efficient. In this work, we have demonstrated a synaptic element based on a magnetic domain wall device. The domain wall motion was controlled with the use of synthetic pinning sites, which were introduced by Boron (B_+) ion-implantation for local modification of the magnetic properties. The magnetization switching process of a Co/Pd multilayer structure with perpendicular magnetic anisotropy was observed by using MagVision Kerr microscopy system. The B_+ implantation depth was controlled by varying the thickness of a Ta overcoat layer. The Kerr microscopy results correlate with the electrical measurements of the wire which show multiple resistive states. The control of the domain wall motion with the synthetic pinning sites is demonstrated to be a reliable technique for neuromorphic applications.

Keywords: neuromorphic computing, domain wall device, domain wall pinning

Introduction:

Artificial intelligence (AI) is gaining significant attention in recent years [1-7]. Current consumer devices such as smartphones and televisions already make use of AI. In these devices, AI algorithms are performed on components which function on a von Neumann architecture, which consume a significant amount of power [8-10]. In contrast, brain-inspired neuromorphic computing (NC) hardware, which consists of a network of synthetic neurons interconnected through synaptic devices and mimics the functions of the brain, is expected to perform complex information processing at low power [11-15]. As a result, NC is gaining significant attention [2, 5, 16]. In an NC system, neurons act as processing elements by taking multiple inputs and generating an output in a programmed way. Synapses, in contrast, transmit signals modulated according to a *weight* to the neurons. This weight is physically stored in the synapse itself which means the synaptic element must be non-volatile in nature. Synapses can thus be considered as the memory element of a neuromorphic device. Weights can be changed externally by modifying specific properties of the synapses until the system performs in an expected way. This is the so-called learning process. The physical implementation of these concepts has been mostly done by using resistive random access memory (RRAM) [17], phase change RAM (PCRAM) [18-20], and ferroelectric RAM (FeRAM) [21, 22] devices. Recently, RRAM is gaining more attention, due to its smaller cell size and lower energy consumption. The multiple states are achieved by the excellent control the amount of oxygen vacancy generated in the conducting filament regions [23]. The device-to-device variability is one of the major bottlenecks of RRAM [24].

Recent discoveries in the field of spintronics have opened new possibilities for ultra-low power implementation of neuromorphic devices. In 2016, Abhronil *et al*. firstly proposed a spintronic-based device able to mimic the functionality of both neurons and synapses [25]. The device consists of a magnetic tunnel junction (MTJ) where the free layer (a ferromagnet whose magnetization can be manipulated) is separated from the pinned layer (a ferromagnet whose magnetization is fixed) by a tunnelling oxide layer. The free layer consists of two oppositely polarized magnetic domains separated by a domain wall (DW). In the case of a synapse, the weight is stored by the mere position of the domain wall. The domain wall position can be modulated by spin-orbit torque (SOT) or spin-transfer torque (STT) mechanisms [26]. The magnitude of the read voltage is modulated by the device resistance which, in turn, depends on the domain wall position in the free layer of the MTJ. The velocity of domain wall motion has been reported to be about several hundred meter per second to 1000 meter per second [27, 28]. Therefore, such devices can be operated in GHz mode with energy consumption below pJ [10, 26].

Co/Ni multilayers based MTJ devices, which perform as synaptic elements, have also been investigated for neuromorphic computing by Borders *et al.* [29]. However, it is unclear if the domain wall propagation in these devices is controllable. In this connection, we have investigated magnetic wires made of Co/Pd multilayers with synthetic pinning sites as a potential candidate for neuromorphic computing. Ion-implantation was employed to locally modify the magnetic properties in order to control domain wall pinning effectively. We have demonstrated multiple resistive states by performing magnetoresistance measurements.

Experimental details:

Co/Pd multilayers of the type shown in Fig. 1(a) were prepared by DC magnetron sputtering. All the samples have a Ta cap layer to prevent the samples from oxidation. Ion-implantation was carried out using B^+ ions with an energy of 10 keV and an ion dose of 5×10^{15} ions/cm^2. The implantation dose along the depth was controlled by varying the thickness of an additional Ta overcoat, ranging from 0 to 6 nm. The samples are named as deep-implantation (DI), medium-implantation (MI) and shallow-implantation (DI), corresponding the thickness of Ta overcoat layer, t_{Ta} = 0 nm, 3 nm and 6 nm. Magnetic properties of the films were measured by vibrating sample magnetometer (VSM) along in-plane (IP) and out-of-plane (OOP) directions. At first, the Co/Pd wires were fabricated by E-beam lithography, followed by ion-milling. For the formation of pinning sites, an additional lithography step was carried out. Through the trenches of the resist, a Ta overcoat layer with the thickness of 6 nm, 3 nm and 0 nm, was deposited to control the depth of the B_+ implanted into Co/Pd devices. Hysteresis measurement and domain imaging of the wires were carried out using Kerr microscope. Magnetoresistance was measured by passing a DC current while sweeping the magnetic field and imaging the domains simultaneously.

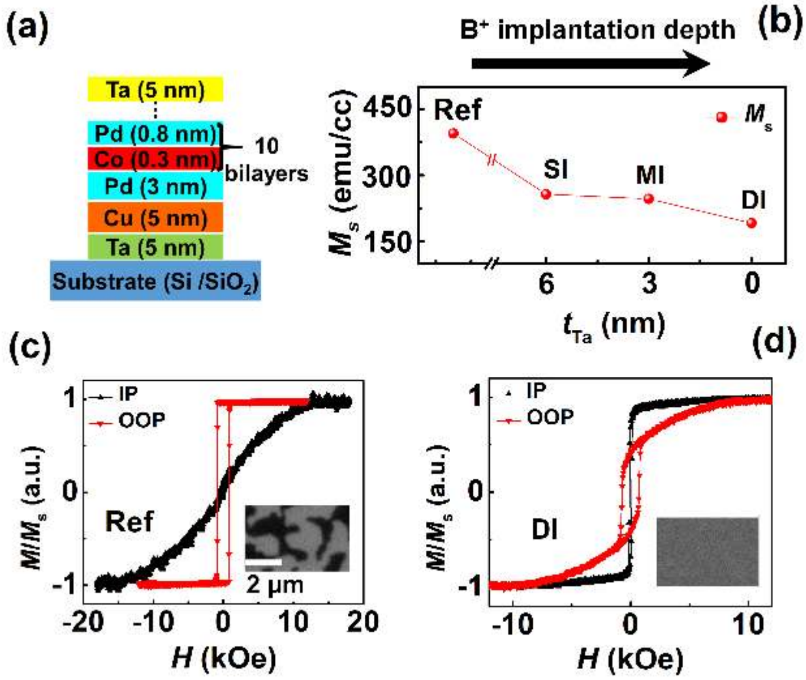

Figure 1. (a) Schematic illustration of the sample structure. (b) The saturation magnetization M_s as a function of the Ta overcoat layer thickness t_{Ta}, such as 6 nm, 3 nm and 0 nm, which is defined as shallow-implantation (SI), medium-implantation (MI) and deep-implantation (DI) respectively based on the depth of B_+ implantation. The arrow shows the B_+ implantation depth. In-plane (IP) and out-of-plane (OOP) hysteresis loops of (c) reference sample without B_+ implantation (named as Ref) and (d) DI sample with deep-implantation. The insets show the magnetic domains of the samples at demagnetized state.

Results and discussion:

At first, properties of the deposited film (before the lithography step) with different B_+ implantation depth were characterized. Figure 1(b) shows the saturation magnetization M_s (measured at 12 kOe) of Co/Pd thin films as a function of t_{Ta}. The reference sample (Ref), without implantation, shows the highest M_s. As the t_{Ta} reduces, the depth of B_+ implantation increases and the M_s reduces. The DI sample shows the lowest M_s. Hysteresis loops of the Ref and DI samples along IP and OOP directions are shown in Fig. 1(c) and (d). The Ref sample exhibits a clear perpendicular magnetic anisotropy (PMA), which is observed from the perfect square loops along OOP, while for the DI sample, IP direction shows the square loop, indicating a loss of PMA. The insets show the magnetic domain patterns of the corresponding samples. The Ref sample shows large domains, where the grey and black patterns indicate the up and down domains, respectively. This is an indication of PMA in this sample. For DI sample, the domains vanish, indicating a lack of PMA, which is associated with a decrease in anisotropy energy K_u with ion implantation [30-32]. These results indicate that the B_+ implantation is able to modify the magnetic properties of Co/Pd multilayer and that the implantation depth can be controlled by changing the Ta overcoat thickness [33-36].

After the lithography process, the wire properties were measured. Figure 2(a) shows a schematic of the domain wall microwire. The red and blue colors indicate up and down magnetized domains, respectively. The B_+ implanted regions are shown in yellow, with widths of 400 nm, 600 nm, 800 nm and 1 μm from left to right. Figure 2(b) shows the hysteresis loops of the microwire device with 1μm width and 15 μm length, which was measured by using MagVision Kerr microscopy system. The Ref sample shows a steep hysteresis loop, indicating that the magnetization reverses by a swift motion of the domain wall in a narrow range of applied magnetic field. However, for samples implanted with B_+, the magnetization shows multiple steps, indicating that the domain wall propagation is hindered by the pinning sites. For these samples, the loops also become wider, indicating the presence of domain wall pinning at the implanted regions. This behaviour is also reflected in the switching field distribution (SFD) shown in Fig. 2(c), by calculating the ratio $\Delta H/H_c$, where ΔH is the difference between the nucleation field and saturation field and H_c is the coercivity [37, 38].

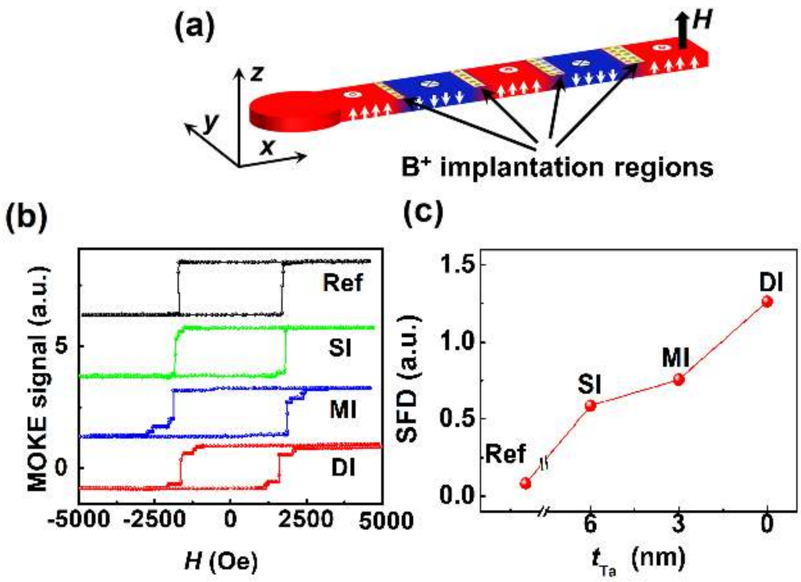

Figure 2. (a) Schematic view of the domain wall microwire. The yellow regions are implantation area, which length is 400 nm, 600 nm, 800 nm and 1 μm from left to right. (b) Hysteresis loops of the microwire device with different depth of B_+ implantation. (c) The switching field distribution (SFD) as a function of t_{Ta} for the microwire devices.

Figure 3 shows the domain wall devices with 1 μm width and 15 μm length. The circular region with a diameter of 5 μm at the left side was introduced to nucleate domain wall. To visualize the domain wall propagation and to understand the pinning effect, we captured the images of the domain patterns at different values of the applied magnetic field. It can be noticed that the Ref sample shows a grey colored domain (representing positive magnetization) until a reversal field of about –1854 Oe was applied. When the magnitude of the reversal field was increased to –1858 Oe, the magnetization of the whole wire reversed. The presence of a single black colored domain, representing a negative magnetization, is an indication of a swift magnetization reversal caused by domain wall propagation throughout the whole device without pinning. Such a magnetization reversal led to the observation of a sharp hysteresis loop in Fig. 2(b) and a low SFD in Fig. 2(c) for the Ref sample.

For the SI sample, however, the magnetization reversal occurs in a narrow range of field around –1418 Oe. Since Co/Pd multilayers have an anisotropy field of over 10 kOe, this reversal at low fields is caused by nucleation of a small region where the reversal field is much lower than the anisotropy field. Such a reversal is reported to be caused by defects which arise due to many reasons, one of them being local non-uniformity in the layer thickness of Co and Pd [39]. However, it is interesting to note that this reversed domain did not propagate uncontrollably as in the reference sample but is stopped at the two edges where B_+ implantation was carried out. This result indicates that the regions where B_+ was implanted can act as pinning centres. When the reversal field was increased to –1750 Oe, the left region of the device reversed its magnetization. A sufficiently strong field of –1941 Oe was required to reverse the entire device. Such a magnetization reversal in steps resulted in the observation of a wider and stepped hysteresis loop and a larger SFD for this sample in Fig. 2(b) and (c), respectively.

In Fig. 3(c), we show the magnetization reversal in the DI sample, which has the deepest implantation of B_+. In this sample, each region separated by pinning sites reverses individually, indicating that the pinning strength is high in this sample. Every region, implanted with B_+ ions, hinders the domain wall propagation and offers effective pinning. The above-described behaviour explains why the hysteresis loop in Fig. 2(b) exhibited many steps and a larger SFD, as observed in Fig. 2(c). These results indicate that B_+ implantation through a resist mask is a useful technique to achieve effective DW pinning.

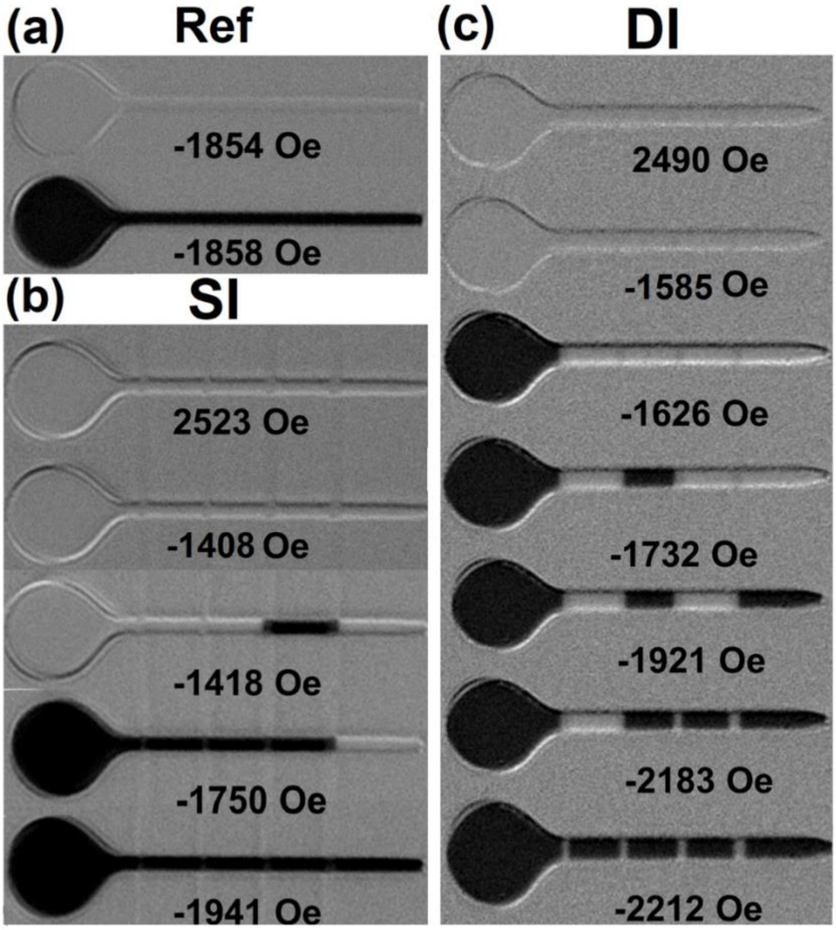

Figure 3. Differential Kerr images at the different magnetic field for (a) reference sample (Ref) and (b) SI and (c) DI samples with Ta overcoat layer with the thickness of $t_{Ta} = 6$ and $t_{Ta} = 0$ nm. The grey colour represents the domain with positive magnetization and the black colour the domain with negative magnetization. The devices with 1 µm width and 15 µm length.

In order to measure the potential of such a device for neuromorphic computing applications, we measured the resistance of the device at several magnetic fields. For synaptic devices, multiple resistive states are required. Switching between these multiple resistive states is expected to be achieved by spin-torque currents. However, for this preliminary study, we measured the resistance of the devices as a function of the applied external magnetic field. Figure 4(a) shows the schematic of the experimental setup. A DC current of 700 µA was sent through the device and the magnetoresistance along the wire was measured while sweeping the external magnetic field.

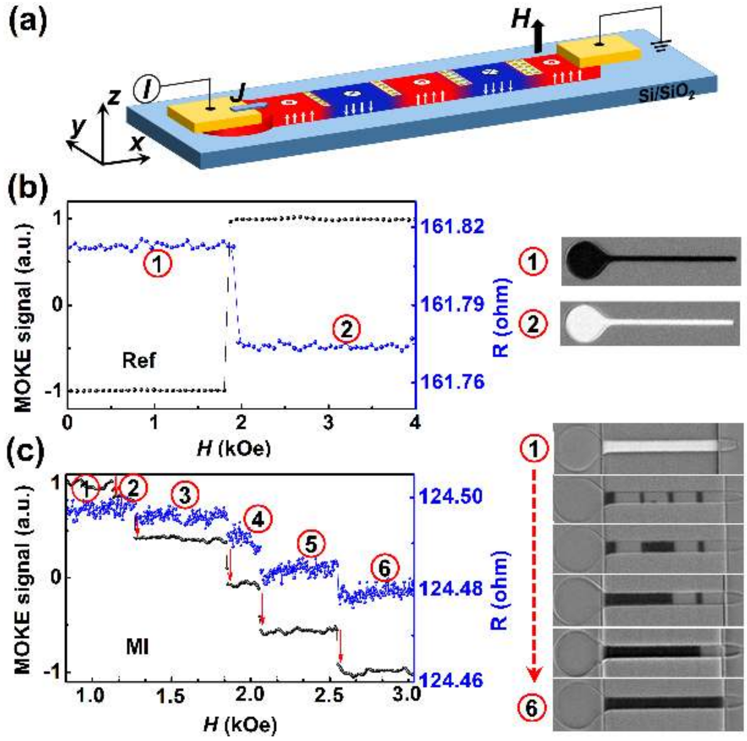

Figure 4. (a) Schematic of the setup used for magnetoresistance measurement for devices with 1 μm width and 15 μm length. The resistance change with respect to the magnetic field, as well as the MOKE signal change for (b) reference (Ref) sample and (c) mediate-implantation (MI) sample.

Figure 4(b) shows the variation of MOKE signal and resistance as a function of a magnetic field for the Ref sample. It can be noticed that the magnetization of the whole device reverses together and hence two resistive states are observed. However, the MI samples in Fig. 4(c) shows multiple resistive states. The snapshots of the domain configuration at the corresponding magnetic field show clear switching of individual magnetic domains. A slight positive slope in the resistance as a function of time is an indication of Joule heating. It can be noticed that there is a distinct change in the resistance besides the positive slope, which confirms that the change in resistance is due to the different domain states and not due to Joule heating. For neuromorphic computing, the Co/Pd multilayer nanowires with pinning sites will be patterned into crossbar array structure. Switching of such a multilevel resistive state can be achieved by spin-torque current induced domain wall motion. In the future, more layers could be added and a reading mechanism based on tunnel magnetoresistance (TMR) implemented to increase the voltage swing and the difference between voltage levels. These results indicate the promise of nanowires with synthetic pinning sites for synaptic device applications.

Conclusions:

We have demonstrated a synaptic element using a magnetic DW device with PMA. The DW propagation was controlled utilizing synthetic pinning sites that were introduced by B_+ implantation. We carried out high-resolution Kerr microscopy measurement, along with resistance measurements, to understand the magnetization switching process and multilevel resistance resistive states. The results in this work show that the domain wall device can be reliably used as a neuromorphic synaptic element.

Acknowledgment:

The authors acknowledge MOE AcRF Tier 1 grant.

References:

[1] Krittanawong C, Zhang H J, Wang Z, Aydar M and Kitai T 2017 *J Am Coll Cardiol.* **69** 2657-2664

[2] Thrall J H, Li X, Li Q Z, Cruz C, Do S, Dreyer K and Brink J 2018 *J Am Coll Radiol.* **15** 504-508

[3] Merk D, Friedrich L, Grisoni F and Schneider G 2018 *Mol. Inform.* **37**

[4] Gaba S, Sheridan P, Zhou J T, Choi S and Lu W 2013 *Nanoscale* **5** 5872-8

[5] Silver D, Huang A, Maddison C J, Guez A, Sifre L, Van den Driessche G, Schrittwieser J, Antonoglou I, Panneershelvam V, Lanctot M, Dieleman S, Grewe D, Nham J, Kalchbrenner N, Sutskever I, Lillicrap T, Leach M, Kavukcuoglu K, Graepel T and Hassabis D 2016 *Nature* **529** 484

[6] Mellit A, Kalogirou S A. 2008 *Prog. Energy Combust. Sci.* **34** 574-632

[7] Raza M Q, Khosravi A 2015 *Renewable & Sustainable Energy Reviews* **50** 1352-72

[8] Aly M M S, Gao M Y, Hills G, Lee C S, Pitner G, Shulaker M M, Wu T F, Asheghi M, Bokor J, Franchetti F, Goodson K E, Kozyrakis C, Markov I, Olukotun K, Pileggi L, Pop E, Rabaey J, Re C, Wong H S P and Mitra S 2015 *Computer* **48** 24-33

[9] Gonzalez R, Horowitz M. 1996. *IEEE J. Solid-State Circuits* **31** 1277-84

[10] Bhatti S, Sbiaa R, Hirohata A, Ohno H, Fukami S and Piramanayagam S N 2017 *Mater. Today* **20** 530-48

[11] Sidler S, Boybat I, Shelby R M, Narayanan P, Jang J, *et al.* 2016 In *2016 46th European Solid-State Device Research Conference*.

[12] Hwang C S. 2015 *Adv. Electron. Mater.* **1** 1400056

[13] Wolfert S, Ge L, Verdouw C and Bogaardt M J 2017 *Agric. Sys.* **153** 69-80

[14] Irmanova A, James A P 2018 *Analog Integr. Circuits Signal Process* **95** 429-34

[15] Van de Burgt Y, Lubberman E, Fuller E J, Keene S T, Faria G C, Agarwal S, Marinella M J, Talin A A and Salleo A 2017 *Nat. Mater.* **16** 414

[16] Merced-Grafals E J, Davila N, Ge N, Williams R S, Strachan J P 2016 *Nanotechnology* **27** 365202

[17] Ielmini D *Microelectron. Eng.* **190** 10

[18] Wright C D, Hosseini P and Diosdado J A V 2013 *Adv. Funct. Mater.* **23** 2248-54

[19] Nandakumar S R, Le Gallo M, Boybat I, Rajendran B, Sebastian A and Eleftheriou E 2018 *J. Appl. Phys.* **124** 152135

[20] Wang L, Lu S R and Wen J 2017 *Nanoscale Res. Lett.* **12** 347

[21] Ishiwara H. 2012 *Curr. Appl. Phys.* **12** 603-11

[22] Scott J F, Dearaujo C A P 1989 *Science* **246** 1400-5

[23] Hong X, Loy D J, Dananjaya P A, Tan F, Ng C and Lew W 2018 *J. Mater. Sci.* **53**, 8720-8746

[24] Waser R and Aono M 2007 *Nat. Mater.* **6**, 833–840

[25] Sengupta A, Panda P, Wijesinghe P, Kim Y and Roy K 2016 *Sci. Rep.* **6** 30039

[26] Ramaswamy R, Lee J M, Cai K and Yang H 2018 *Appl. Phys. Rev.* **5**, 031107

[27] Parkin S and Yang S H 2015 *Nat. Nanotechnol.* **10**, 195-198

[28] Yang S H, Ryu K S, Parkin S 2015 *Nat. Nanotechnol.* **10,** 221-216

[29] Borders W A, Akima H, Fukami S, Moriya S, Kurihara S, Horio Y, Sato S and Ohno H 2017 *Appl. Phys. Express* **10** 013007

[30] Sbiaa R, Ranjbar M and Åkerman J 2015 *J. Appl. Phys.* **117** 17C102

[31] Sbiaa R, Shaw J M, Nembach H T, Al Bahri M, Ranjbar M, Åkerman J and Piramanayagam S N 2016 *J. Phys. D Appl. Phys.* **49** 425002

[32] Liu LW, Sheng W, Bai J M, Cao J W, Lou Y F, Wang Y, Wei F L and Lu J 2012 *Appl. Surf. Sci.* **258** 8124-7

[33] Gaur N, Pandey K K M, Maurer S L, Piramanayagam S N, Nunes R W, Yang H and Bhatia C S 2011 *J. Appl. Phys.* **110** 083917

[34] Gaur N, Piramanayagam S N, Maurer S L, Nunes R W, Steen S, Yang H and Bhatia C S 2011 *J. Phys. D Appl. Phys.* **44** 365001

[35] Krichevsky A, Lavrenov A, Amos N, Hu B, Taylor K and Khizroev S. 2008 *J. Nanoelectron. Optoelectron* **3** 274-6

[36] Jin T L, Kumar D, Gan W L, Ranjbar M, Luo F L, Sbiaa R, Liu X X, Lew W S and Piramanayagam S N 2018 *Phys. Status Solidi RRL* **2018** 1800197

[37] Berger A, Xu Y, Lengsfield B, Ikeda Y and Fullerton E E 2005 *IEEE Trans. Magn.* **41** 3178-80

[38] Berger A, Lengsfield B, Ikeda Y. 2006 *J. Appl. Phys.* **99** 08E705

[39] Speetzen N, Stadler B, Yuan E, Victora R H, Qi X, Judy J H, Supper N and Pohkil T 2005 *J. Magn. Magn. Mater.* **287** 181-7